

PDF hosted at the Radboud Repository of the Radboud University Nijmegen

The following full text is a preprint version which may differ from the publisher's version.

For additional information about this publication click this link.

<http://hdl.handle.net/2066/75121>

Please be advised that this information was generated on 2018-07-08 and may be subject to change.

Measurement of trilinear gauge boson couplings from $WW + WZ \rightarrow \ell\nu jj$ events in $p\bar{p}$ collisions at $\sqrt{s} = 1.96$ TeV

V.M. Abazov³⁷, B. Abbott⁷⁵, M. Abolins⁶⁵, B.S. Acharya³⁰, M. Adams⁵¹, T. Adams⁴⁹, E. Aguilo⁶, M. Ahsan⁵⁹, G.D. Alexeev³⁷, G. Alkhazov⁴¹, A. Alton^{64,a}, G. Alverson⁶³, G.A. Alves², L.S. Ancu³⁶, M.S. Anzelc⁵³, M. Aoki⁵⁰, Y. Arnoud¹⁴, M. Arov⁶⁰, M. Arthaud¹⁸, A. Askew^{49,b}, B. Åsman⁴², O. Atramentov^{49,b}, C. Avila⁸, J. BackusMayes⁸², F. Badaud¹³, L. Bagby⁵⁰, B. Baldin⁵⁰, D.V. Bandurin⁵⁹, S. Banerjee³⁰, E. Barberis⁶³, A.-F. Barfuss¹⁵, P. Bargassa⁸⁰, P. Baringer⁵⁸, J. Barreto², J.F. Bartlett⁵⁰, U. Bassler¹⁸, D. Bauer⁴⁴, S. Beale⁶, A. Bean⁵⁸, M. Begalli³, M. Biegel⁷³, C. Belanger-Champagne⁴², L. Bellantoni⁵⁰, A. Bellavance⁵⁰, J.A. Benitez⁶⁵, S.B. Beri²⁸, G. Bernardi¹⁷, R. Bernhard²³, I. Bertram⁴³, M. Besançon¹⁸, R. Beuselinck⁴⁴, V.A. Bezzubov⁴⁰, P.C. Bhat⁵⁰, V. Bhatnagar²⁸, G. Blazey⁵², S. Blessing⁴⁹, K. Bloom⁶⁷, A. Boehnlein⁵⁰, D. Boline⁶², T.A. Bolton⁵⁹, E.E. Boos³⁹, G. Borissov⁴³, T. Bose⁶², A. Brandt⁷⁸, R. Brock⁶⁵, G. Brooijmans⁷⁰, A. Bross⁵⁰, D. Brown¹⁹, X.B. Bu⁷, D. Buchholz⁵³, M. Buehler⁸¹, V. Buescher²², V. Bunichev³⁹, S. Burdin^{43,c}, T.H. Burnett⁸², C.P. Buszello⁴⁴, P. Calfayan²⁶, B. Calpas¹⁵, S. Calvet¹⁶, J. Cammin⁷¹, M.A. Carrasco-Lizarraga³⁴, E. Carrera⁴⁹, W. Carvalho³, B.C.K. Casey⁵⁰, H. Castilla-Valdez³⁴, S. Chakrabarti⁷², D. Chakraborty⁵², K.M. Chan⁵⁵, A. Chandra⁴⁸, E. Cheu⁴⁶, D.K. Cho⁶², S.W. Cho³², S. Choi³³, B. Choudhary²⁹, T. Christoudias⁴⁴, S. Cihangir⁵⁰, D. Claes⁶⁷, J. Clutter⁵⁸, M. Cooke⁵⁰, W.E. Cooper⁵⁰, M. Corcoran⁸⁰, F. Couderc¹⁸, M.-C. Cousinou¹⁵, D. Cutts⁷⁷, M. Ćwiok³¹, A. Das⁴⁶, G. Davies⁴⁴, K. De⁷⁸, S.J. de Jong³⁶, E. De La Cruz-Burelo³⁴, K. DeVaughan⁶⁷, F. Déliot¹⁸, M. Demarteau⁵⁰, R. Demina⁷¹, D. Denisov⁵⁰, S.P. Denisov⁴⁰, S. Desai⁵⁰, H.T. Diehl⁵⁰, M. Diesburg⁵⁰, A. Dominguez⁶⁷, T. Dorland⁸², A. Dubey²⁹, L.V. Dudko³⁹, L. Duflot¹⁶, D. Duggan⁴⁹, A. Duperrin¹⁵, S. Dutt²⁸, A. Dyshkant⁵², M. Eads⁶⁷, D. Edmunds⁶⁵, J. Ellison⁴⁸, V.D. Elvira⁵⁰, Y. Enari⁷⁷, S. Eno⁶¹, M. Escalier¹⁵, H. Evans⁵⁴, A. Evdokimov⁷³, V.N. Evdokimov⁴⁰, G. Facini⁶³, A.V. Ferapontov⁵⁹, T. Ferbel^{61,71}, F. Fiedler²⁵, F. Filthaut³⁶, W. Fisher⁵⁰, H.E. Fisk⁵⁰, M. Fortner⁵², H. Fox⁴³, S. Fu⁵⁰, S. Fuess⁵⁰, T. Gadfort⁷⁰, C.F. Galea³⁶, A. Garcia-Bellido⁷¹, V. Gavrilov³⁸, P. Gay¹³, W. Geist¹⁹, W. Geng^{15,65}, C.E. Gerber⁵¹, Y. Gershtein^{49,b}, D. Gillberg⁶, G. Ginther^{50,71}, B. Gómez⁸, A. Goussiou⁸², P.D. Grannis⁷², S. Greder¹⁹, H. Greenlee⁵⁰, Z.D. Greenwood⁶⁰, E.M. Gregores⁴, G. Grenier²⁰, Ph. Gris¹³, J.-F. Grivaz¹⁶, A. Grohsjean¹⁸, S. Grünendahl⁵⁰, M.W. Grünewald³¹, F. Guo⁷², J. Guo⁷², G. Gutierrez⁵⁰, P. Gutierrez⁷⁵, A. Haas⁷⁰, P. Haefner²⁶, S. Hagopian⁴⁹, J. Haley⁶⁸, I. Hall⁶⁵, R.E. Hall⁴⁷, L. Han⁷, K. Harder⁴⁵, A. Harel⁷¹, J.M. Hauptman⁵⁷, J. Hays⁴⁴, T. Hebbeker²¹, D. Hedin⁵², J.G. Hegeman³⁵, A.P. Heinson⁴⁸, U. Heintz⁶², C. Hensel²⁴, I. Heredia-De La Cruz³⁴, K. Herner⁶⁴, G. Hesketh⁶³, M.D. Hildreth⁵⁵, R. Hirosky⁸¹, T. Hoang⁴⁹, J.D. Hobbs⁷², B. Hoeneisen¹², M. Hohlfield²², S. Hossain⁷⁵, P. Houben³⁵, Y. Hu⁷², Z. Hubacek¹⁰, N. Huske¹⁷, V. Hynek¹⁰, I. Iashvili⁶⁹, R. Illingworth⁵⁰, A.S. Ito⁵⁰, S. Jabeen⁶², M. Jaffré¹⁶, S. Jain⁷⁵, K. Jakobs²³, D. Jamin¹⁵, R. Jesik⁴⁴, K. Johns⁴⁶, C. Johnson⁷⁰, M. Johnson⁵⁰, D. Johnston⁶⁷, A. Jonckheere⁵⁰, P. Jonsson⁴⁴, A. Juste⁵⁰, E. Kajfasz¹⁵, D. Karmanov³⁹, P.A. Kasper⁵⁰, I. Katsanos⁶⁷, V. Kaushik⁷⁸, R. Kehoe⁷⁹, S. Kermiche¹⁵, N. Khalatyan⁵⁰, A. Khanov⁷⁶, A. Kharchilava⁶⁹, Y.N. Khazdheev³⁷, D. Khatidze⁷⁷, M.H. Kirby⁵³, M. Kirsch²¹, B. Klima⁵⁰, J.M. Kohli²⁸, J.-P. Konrath²³, A.V. Kozelov⁴⁰, J. Kraus⁶⁵, T. Kuhl²⁵, A. Kumar⁶⁹, A. Kupco¹¹, T. Kurča²⁰, V.A. Kuzmin³⁹, J. Kvita⁹, F. Lacroix¹³, D. Lam⁵⁵, S. Lammers⁵⁴, G. Landsberg⁷⁷, P. Lebrun²⁰, H.S. Lee³², W.M. Lee⁵⁰, A. Leflat³⁹, J. Lellouch¹⁷, L. Li⁴⁸, Q.Z. Li⁵⁰, S.M. Lietti⁵, J.K. Lim³², D. Lincoln⁵⁰, J. Linnemann⁶⁵, V.V. Lipaev⁴⁰, R. Lipton⁵⁰, Y. Liu⁷, Z. Liu⁶, A. Lobodenko⁴¹, M. Lokajicek¹¹, P. Love⁴³, H.J. Lubatti⁸², R. Luna-Garcia^{34,d}, A.L. Lyon⁵⁰, A.K.A. Maciel², D. Mackin⁸⁰, P. Mättig²⁷, R. Magaña-Villalba³⁴, P.K. Mal⁴⁶, S. Malik⁶⁷, V.L. Malyshev³⁷, Y. Maravin⁵⁹, B. Martin¹⁴, R. McCarthy⁷², C.L. McGivern⁵⁸, M.M. Meijer³⁶, A. Melnitchouk⁶⁶, L. Mendoza⁸, D. Menezes⁵², P.G. Mercadante⁵, M. Merkin³⁹, K.W. Merritt⁵⁰, A. Meyer²¹, J. Meyer²⁴, N.K. Mondal³⁰, R.W. Moore⁶, T. Moulik⁵⁸, G.S. Muanza¹⁵, M. Mulhearn⁷⁰, O. Mundal²², L. Mundim³, E. Nagy¹⁵, M. Naimuddin⁵⁰, M. Narain⁷⁷, H.A. Neal⁶⁴, J.P. Negret⁸, P. Neustroev⁴¹, H. Nilsen²³, H. Nogima³, S.F. Novaes⁵, T. Nunnemann²⁶, G. Obrant⁴¹, C. Ochando¹⁶, D. Onoprienko⁵⁹, J. Orduna³⁴, N. Oshima⁵⁰, N. Osman⁴⁴, J. Osta⁵⁵, R. Otec¹⁰, G.J. Otero y Garzón¹, M. Owen⁴⁵, M. Padilla⁴⁸, P. Padley⁸⁰, M. Pangilinan⁷⁷, N. Parashar⁵⁶, S.-J. Park²⁴, S.K. Park³², J. Parsons⁷⁰, R. Partridge⁷⁷, N. Parua⁵⁴, A. Patwa⁷³, B. Penning²³, M. Perfilov³⁹, K. Peters⁴⁵, Y. Peters⁴⁵, P. Pétróff¹⁶, R. Piegaia¹, J. Piper⁶⁵, M.-A. Pleier²², P.L.M. Podesta-Lerma^{34,e}, V.M. Podstavkov⁵⁰, Y. Pogorelov⁵⁵, M.-E. Pol², P. Polozov³⁸, A.V. Popov⁴⁰, M. Prewitt⁸⁰, S. Protopopescu⁷³, J. Qian⁶⁴, A. Quadt²⁴, B. Quinn⁶⁶, A. Rakitine⁴³, M.S. Rangel¹⁶, K. Ranjan²⁹, P.N. Ratoff⁴³, P. Renkel⁷⁹, P. Rich⁴⁵, M. Rijssenbeek⁷², I. Ripp-Baudot¹⁹, F. Rizatdinova⁷⁶, S. Robinson⁴⁴, M. Rominsky⁷⁵, C. Royon¹⁸, P. Rubinov⁵⁰, R. Ruchti⁵⁵, G. Safronov³⁸, G. Sajot¹⁴, A. Sánchez-Hernández³⁴, M.P. Sanders²⁶, B. Sanghi⁵⁰, G. Savage⁵⁰, L. Sawyer⁶⁰, T. Scanlon⁴⁴, D. Schaile²⁶, R.D. Schamberger⁷², Y. Scheglov⁴¹, H. Schellman⁵³, T. Schliephake²⁷, S. Schlobohm⁸², C. Schwanenberger⁴⁵, R. Schwienhorst⁶⁵,

J. Sekaric⁴⁹, H. Severini⁷⁵, E. Shabalina²⁴, M. Shamim⁵⁹, V. Shary¹⁸, A.A. Shchukin⁴⁰, R.K. Shivpuri²⁹,
V. Siccaldi¹⁹, V. Simak¹⁰, V. Sirotenko⁵⁰, P. Skubic⁷⁵, P. Slattery⁷¹, D. Smirnov⁵⁵, G.R. Snow⁶⁷, J. Snow⁷⁴,
S. Snyder⁷³, S. Söldner-Rembold⁴⁵, L. Sonnenschein²¹, A. Sopczak⁴³, M. Sosebee⁷⁸, K. Soustruznik⁹, B. Spurlock⁷⁸,
J. Stark¹⁴, V. Stolin³⁸, D.A. Stoyanova⁴⁰, J. Strandberg⁶⁴, M.A. Strang⁶⁹, E. Strauss⁷², M. Strauss⁷⁵,
R. Ströhmer²⁶, D. Strom⁵¹, L. Stutte⁵⁰, S. Sumowidagdo⁴⁹, P. Svoisky³⁶, M. Takahashi⁴⁵, A. Tanasijczuk¹,
W. Taylor⁶, B. Tiller²⁶, M. Titov¹⁸, V.V. Tokmenin³⁷, I. Torchiani²³, D. Tsybychev⁷², B. Tuchming¹⁸, C. Tully⁶⁸,
P.M. Tuts⁷⁰, R. Unalan⁶⁵, L. Uvarov⁴¹, S. Uvarov⁴¹, S. Uzunyan⁵², P.J. van den Berg³⁵, R. Van Kooten⁵⁴,
W.M. van Leeuwen³⁵, N. Varelas⁵¹, E.W. Varnes⁴⁶, I.A. Vasilyev⁴⁰, P. Verdier²⁰, L.S. Vertogradov³⁷,
M. Verzocchi⁵⁰, M. Vesterinen⁴⁵, D. Vilanova¹⁸, P. Vint⁴⁴, P. Vokac¹⁰, R. Wagner⁶⁸, H.D. Wahl⁴⁹, M.H.L.S. Wang⁷¹,
J. Warchol⁵⁵, G. Watts⁸², M. Wayne⁵⁵, G. Weber²⁵, M. Weber^{50,f}, L. Welty-Rieger⁵⁴, A. Wenger^{23,g},
M. Wetstein⁶¹, A. White⁷⁸, D. Wicke²⁵, M.R.J. Williams⁴³, G.W. Wilson⁵⁸, S.J. Wimpenny⁴⁸, M. Wobisch⁶⁰,
D.R. Wood⁶³, T.R. Wyatt⁴⁵, Y. Xie⁷⁷, C. Xu⁶⁴, S. Yacoub⁵³, R. Yamada⁵⁰, W.-C. Yang⁴⁵, T. Yasuda⁵⁰,
Y.A. Yatsunenko³⁷, Z. Ye⁵⁰, H. Yin⁷, K. Yip⁷³, H.D. Yoo⁷⁷, S.W. Youn⁵⁰, J. Yu⁷⁸, C. Zeitnitz²⁷, S. Zelitch⁸¹,
T. Zhao⁸², B. Zhou⁶⁴, J. Zhu⁷², M. Zielinski⁷¹, D. Zieminska⁵⁴, L. Zivkovic⁷⁰, V. Zutshi⁵², and E.G. Zverev³⁹

(The DØ Collaboration)

¹Universidad de Buenos Aires, Buenos Aires, Argentina

²LAFEX, Centro Brasileiro de Pesquisas Físicas, Rio de Janeiro, Brazil

³Universidade do Estado do Rio de Janeiro, Rio de Janeiro, Brazil

⁴Universidade Federal do ABC, Santo André, Brazil

⁵Instituto de Física Teórica, Universidade Estadual Paulista, São Paulo, Brazil

⁶University of Alberta, Edmonton, Alberta, Canada; Simon Fraser University,
Burnaby, British Columbia, Canada; York University, Toronto,
Ontario, Canada and McGill University, Montreal, Quebec, Canada

⁷University of Science and Technology of China, Hefei, People's Republic of China

⁸Universidad de los Andes, Bogotá, Colombia

⁹Center for Particle Physics, Charles University,

Faculty of Mathematics and Physics, Prague, Czech Republic

¹⁰Czech Technical University in Prague, Prague, Czech Republic

¹¹Center for Particle Physics, Institute of Physics,
Academy of Sciences of the Czech Republic, Prague, Czech Republic

¹²Universidad San Francisco de Quito, Quito, Ecuador

¹³LPC, Université Blaise Pascal, CNRS/IN2P3, Clermont, France

¹⁴LPSC, Université Joseph Fourier Grenoble 1, CNRS/IN2P3,
Institut National Polytechnique de Grenoble, Grenoble, France

¹⁵CPPM, Aix-Marseille Université, CNRS/IN2P3, Marseille, France

¹⁶LAL, Université Paris-Sud, IN2P3/CNRS, Orsay, France

¹⁷LPNHE, IN2P3/CNRS, Universités Paris VI and VII, Paris, France

¹⁸CEA, Irfu, SPP, Saclay, France

¹⁹IPHC, Université de Strasbourg, CNRS/IN2P3, Strasbourg, France

²⁰IPNL, Université Lyon 1, CNRS/IN2P3, Villeurbanne, France and Université de Lyon, Lyon, France

²¹III. Physikalisches Institut A, RWTH Aachen University, Aachen, Germany

²²Physikalisches Institut, Universität Bonn, Bonn, Germany

²³Physikalisches Institut, Universität Freiburg, Freiburg, Germany

²⁴II. Physikalisches Institut, Georg-August-Universität Göttingen, Göttingen, Germany

²⁵Institut für Physik, Universität Mainz, Mainz, Germany

²⁶Ludwig-Maximilians-Universität München, München, Germany

²⁷Fachbereich Physik, University of Wuppertal, Wuppertal, Germany

²⁸Panjab University, Chandigarh, India

²⁹Delhi University, Delhi, India

³⁰Tata Institute of Fundamental Research, Mumbai, India

³¹University College Dublin, Dublin, Ireland

³²Korea Detector Laboratory, Korea University, Seoul, Korea

³³SungKyunKwan University, Suwon, Korea

³⁴CINVESTAV, Mexico City, Mexico

³⁵FOM-Institute NIKHEF and University of Amsterdam/NIKHEF, Amsterdam, The Netherlands

³⁶Radboud University Nijmegen/NIKHEF, Nijmegen, The Netherlands

³⁷Joint Institute for Nuclear Research, Dubna, Russia

³⁸Institute for Theoretical and Experimental Physics, Moscow, Russia

³⁹Moscow State University, Moscow, Russia

⁴⁰Institute for High Energy Physics, Protvino, Russia

- ⁴¹ Petersburg Nuclear Physics Institute, St. Petersburg, Russia
⁴² Stockholm University, Stockholm, Sweden, and Uppsala University, Uppsala, Sweden
⁴³ Lancaster University, Lancaster, United Kingdom
⁴⁴ Imperial College, London, United Kingdom
⁴⁵ University of Manchester, Manchester, United Kingdom
⁴⁶ University of Arizona, Tucson, Arizona 85721, USA
⁴⁷ California State University, Fresno, California 93740, USA
⁴⁸ University of California, Riverside, California 92521, USA
⁴⁹ Florida State University, Tallahassee, Florida 32306, USA
⁵⁰ Fermi National Accelerator Laboratory, Batavia, Illinois 60510, USA
⁵¹ University of Illinois at Chicago, Chicago, Illinois 60607, USA
⁵² Northern Illinois University, DeKalb, Illinois 60115, USA
⁵³ Northwestern University, Evanston, Illinois 60208, USA
⁵⁴ Indiana University, Bloomington, Indiana 47405, USA
⁵⁵ University of Notre Dame, Notre Dame, Indiana 46556, USA
⁵⁶ Purdue University Calumet, Hammond, Indiana 46323, USA
⁵⁷ Iowa State University, Ames, Iowa 50011, USA
⁵⁸ University of Kansas, Lawrence, Kansas 66045, USA
⁵⁹ Kansas State University, Manhattan, Kansas 66506, USA
⁶⁰ Louisiana Tech University, Ruston, Louisiana 71272, USA
⁶¹ University of Maryland, College Park, Maryland 20742, USA
⁶² Boston University, Boston, Massachusetts 02215, USA
⁶³ Northeastern University, Boston, Massachusetts 02115, USA
⁶⁴ University of Michigan, Ann Arbor, Michigan 48109, USA
⁶⁵ Michigan State University, East Lansing, Michigan 48824, USA
⁶⁶ University of Mississippi, University, Mississippi 38677, USA
⁶⁷ University of Nebraska, Lincoln, Nebraska 68588, USA
⁶⁸ Princeton University, Princeton, New Jersey 08544, USA
⁶⁹ State University of New York, Buffalo, New York 14260, USA
⁷⁰ Columbia University, New York, New York 10027, USA
⁷¹ University of Rochester, Rochester, New York 14627, USA
⁷² State University of New York, Stony Brook, New York 11794, USA
⁷³ Brookhaven National Laboratory, Upton, New York 11973, USA
⁷⁴ Langston University, Langston, Oklahoma 73050, USA
⁷⁵ University of Oklahoma, Norman, Oklahoma 73019, USA
⁷⁶ Oklahoma State University, Stillwater, Oklahoma 74078, USA
⁷⁷ Brown University, Providence, Rhode Island 02912, USA
⁷⁸ University of Texas, Arlington, Texas 76019, USA
⁷⁹ Southern Methodist University, Dallas, Texas 75275, USA
⁸⁰ Rice University, Houston, Texas 77005, USA
⁸¹ University of Virginia, Charlottesville, Virginia 22901, USA and
⁸² University of Washington, Seattle, Washington 98195, USA

(Dated: July 24, 2009)

We present a direct measurement of trilinear gauge boson couplings at γWW and ZWW vertices in WW and WZ events produced in $p\bar{p}$ collisions at $\sqrt{s} = 1.96$ TeV. We consider events with one electron or muon, missing transverse energy, and at least two jets. The data were collected using the D0 detector and correspond to 1.1 fb^{-1} of integrated luminosity. Considering two different relations between the couplings at the γWW and ZWW vertices, we measure these couplings at 68% C.L. to be $\kappa_\gamma = 1.07^{+0.26}_{-0.29}$, $\lambda = 0.00^{+0.06}_{-0.06}$, and $g_1^Z = 1.04^{+0.09}_{-0.09}$ in a scenario respecting $SU(2)_L \otimes U(1)_Y$ gauge symmetry and $\kappa = 1.04^{+0.11}_{-0.11}$ and $\lambda = 0.00^{+0.06}_{-0.06}$ in an “equal couplings” scenario.

PACS numbers: 14.70.Fm, 13.40.Em, 13.85.Rm, 14.70.Hp

I. INTRODUCTION

A primary motivation for studying diboson physics is that the production of two weak bosons and their interactions provide tests of the electroweak sector of the standard model (SM) arising from the vertices involving trilinear gauge boson couplings (TGCs) [1]. Any deviation of TGCs from their predicted SM values would be an

indication for new physics [2] and could provide information on a mechanism for electroweak symmetry breaking (EWSB).

The TGCs involving the W boson have been previously probed in WW , $W\gamma$ and WZ production at the Tevatron $p\bar{p}$ Collider [3, 4, 5, 6] and WW production at the CERN e^+e^- collider (LEP) [7, 8, 9, 10], at different center-of-mass energies and luminosities but no devia-

tion from the SM predictions has been observed. The LEP experiments benefit from the full reconstruction of event kinematics in e^+e^- collisions, high signal selection efficiencies and small background contamination. At the Tevatron, despite larger backgrounds and limited ability to fully reconstruct event kinematics, larger collision energies are probed and WZ production can be used to directly probe the ZWW coupling. The study of WW and WZ production at hadron colliders has focused primarily on the purely leptonic final states [3, 4, 11]. In this paper we present a measurement of the $\gamma WW/ZWW$ couplings based on the same dataset used to obtain the recent evidence for semileptonic decays of WW/WZ boson pairs in hadron collisions [12].

As shown in the tree-level diagrams of Fig. 1, TGCs contribute to WW/WZ production via s -channel diagrams. Production of WW via the s -channel process contains both trilinear γWW and ZWW gauge boson vertices. On the other hand, WZ production is sensitive exclusively to the ZWW vertex.

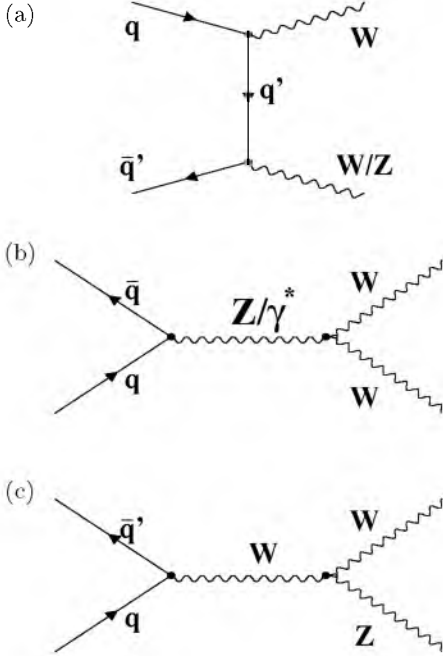


FIG. 1: Tree-level Feynman diagrams for the processes of WW/WZ production at the Tevatron collider via (a) t -channel exchange and (b) and (c) s -channel.

II. PHENOMENOLOGY

Unraveling the origins of EWSB and the mass generation mechanism are currently the highest priorities in particle physics. The SM introduces an effective Higgs potential with an upper limit on the Higgs boson mass of $\simeq 1$ TeV to prevent tree-level unitarity violation [13].

In a Higgs-less scenario or for heavier Higgs boson masses this unitarity limit on the Higgs boson mass indicates the mass scale at which the SM must be superseded by new physics in order to restore unitarity at TeV energies. In this case, the SM is considered to be a low-energy approximation of a general theory. Conversely, if a light Higgs boson exists, the SM may nevertheless be incomplete and new physics could appear at higher energies.

The effects of this general theory can be described by an effective Lagrangian, \mathcal{L}_{eff} , describing low-energy interactions of the new physics at higher energies in a model-independent manner. Expanding in powers of $(1/\Lambda_{NP})$ [14]:

$$\mathcal{L}_{\text{eff}} = \mathcal{L}_{\text{eff}}^{SM} + \sum_{n \geq 1} \sum_i \frac{f_i}{\Lambda_{NP}^n} \mathcal{O}_i^{(n+4)} \quad (1)$$

where $\mathcal{L}_{\text{eff}}^{SM}$ is the $SU(2)_L \times U(1)_Y$ gauge-invariant SM Lagrangian, Λ_{NP} is the energy scale of the new physics and i sums over all operators \mathcal{O}_i of the given energy dimension $(n+4)$. The coefficients f_i parametrize all possible interactions at low energies. Effects of the new physics may not be directly observable because the scale of the new physics is above the energies currently experimentally accessible. However, there could be indirect consequences with measurable effects; for example, on gauge boson interactions.

For the study of gauge boson interactions, the relevant terms in Eq. 1 are those that produce vertices with three or four gauge bosons. The effective Lagrangian, \mathcal{L}_{eff} , that parametrizes the most general Lorentz invariant VWW vertices ($V = Z, \gamma$) involving two W bosons can be defined as [15]

$$\begin{aligned} \frac{\mathcal{L}_{\text{eff}}^{VWW}}{g_{VWW}} = & ig_1^V (W_{\mu\nu}^\dagger W^\mu V^\nu - W_\mu^\dagger V_\nu W^{\mu\nu}) \\ & + i\kappa_V W_\mu^\dagger W_\nu V^{\mu\nu} + i\frac{\lambda_V}{M_W^2} W_\lambda^\dagger W_\mu^\dagger W_\nu^\mu V^{\nu\lambda} \\ & - g_4^V W_\mu^\dagger W_\nu^\dagger (\partial^\mu V^\nu + \partial^\nu V^\mu) \\ & + g_5^V \epsilon^{\mu\nu\lambda\rho} (W_\mu^\dagger \partial_\lambda W_\nu - \partial_\lambda W_\mu^\dagger W_\nu) V_\rho \\ & + i\tilde{\kappa}_V W_\mu^\dagger W_\nu^\dagger \tilde{V}^{\mu\nu} + i\frac{\tilde{\lambda}_V}{M_W^2} W_\lambda^\dagger W_\mu^\dagger W_\nu^\mu \tilde{V}^{\nu\lambda} \end{aligned} \quad (2)$$

where $\epsilon_{\mu\nu\lambda\rho}$ is the fully antisymmetric ϵ tensor, W denotes the W boson field, V denotes the photon or Z boson field, $V_{\mu\nu} = \partial_\mu V_\nu - \partial_\nu V_\mu$, $W_{\mu\nu} = \partial_\mu W_\nu - \partial_\nu W_\mu$, $\tilde{V}_{\mu\nu} = 1/2(\epsilon_{\mu\nu\lambda\rho} V^{\lambda\rho})$, $g_{\gamma WW} = -e$, and $g_{ZWW} = -e \cot \theta_W$, where e is the electron electric charge, θ_W is the weak mixing angle and M_W is the W boson mass. The 14 coupling parameters of VWW vertices are grouped according to the symmetry properties of their corresponding operators: C (charge conjugation) and P (parity) conserving (g_1^V , κ_V , and λ_V), C and P violating but CP conserving (g_5^V), and CP violating (g_4^V , $\tilde{\kappa}_V$, and $\tilde{\lambda}_V$). In the SM all couplings vanish ($g_5^V = g_4^V = \tilde{\kappa}_V = \tilde{\lambda}_V = \lambda_V = 0$) except $g_1^V = \kappa_V = 1$. The value of g_1^γ is fixed by electromagnetic gauge invariance ($g_1^\gamma = 1$) while the value of g_1^Z may differ from its SM value. Considering the C and P conserving couplings only, five couplings remain, and their deviations from the SM values are denoted as

the anomalous TGCs $\Delta g_1^Z = (g_1^Z - 1)$, $\Delta \kappa_\gamma = (\kappa_\gamma - 1)$, $\Delta \kappa_Z = (\kappa_Z - 1)$, λ_γ and λ_Z .

If non zero anomalous TGCs are introduced in Eq. 2, an unphysical increase in the WW and WZ production cross sections will result as the center-of-mass energy, $\sqrt{\hat{s}}$, of the partonic constituents approaches Λ_{NP} . Such divergences would violate unitarity, but can be controlled by introducing a form factor for which the anomalous coupling vanishes as $\hat{s} \rightarrow \infty$:

$$\Delta a(\hat{s}) = \frac{\Delta a_0}{(1 + \hat{s}/\Lambda_{NP}^2)^n} \quad (3)$$

where $n = 2$ for γWW and ZWW couplings, and a_0 is a low-energy approximation of the coupling $a(\hat{s})$. Thus, the previously described anomalous TGCs scale as Δa_0 in Eq. 3. The values of Δa_0 (and a_0) are constrained by requiring the S -matrix unitarity condition that bounds the $J = 1$ partial-wave amplitude of inelastic vector boson scattering by a constant. These constants were derived by Baur and Zeppenfeld [16] for each coupling that contributes to reduced helicity amplitudes in WZ , γW , or WW production via s -channel. Calculated with $M_W = 80$ GeV, $M_Z = 91.1$ GeV and with the dipole form factor as given by Eq. 3, the unitarity bounds for $\Delta \kappa_\gamma$, $\Delta \kappa_Z$, Δg_1^Z and λ TGCs are

$$\begin{aligned} |\Delta \kappa_\gamma^0| &\leq \frac{n^n}{(n-1)^{n-1}} \frac{1.81 \text{ TeV}^2}{\Lambda_{NP}^2}, & |\Delta \lambda_\gamma^0| &\leq \frac{n^n}{(n-1)^{n-1}} \frac{0.96 \text{ TeV}^2}{\Lambda_{NP}^2} \\ |\Delta \kappa_Z^0| &\leq \frac{n^n}{(n-1)^{n-1}} \frac{0.83 \text{ TeV}^2}{\Lambda_{NP}^2}, & |\Delta \lambda_Z^0| &\leq \frac{n^n}{(n-1)^{n-1}} \frac{0.52 \text{ TeV}^2}{\Lambda_{NP}^2} \\ |\Delta g_1^{Z0}| &\leq \frac{n^n}{(n-1)^{n-1}} \frac{0.84 \text{ TeV}^2}{\Lambda_{NP}^2} \end{aligned} \quad (4)$$

For $n = 2$ and $\Lambda_{NP} = 2$ TeV, the unitarity condition sets constraints on the TGCs of $|\Delta \kappa_\gamma^0| \leq 1.81$, $|\Delta \lambda_\gamma^0| \leq 0.96$, $|\Delta \kappa_Z^0| \leq 0.83$, $|\Delta \lambda_Z^0| \leq 0.52$, and $|\Delta g_1^{Z0}| \leq 0.84$. The scale of new physics, Λ_{NP} , was chosen such that the unitarity limits are close to, but no tighter than, the coupling limits set by data. Clearly, as Λ_{NP} increases the effects on anomalous TGCs decrease and their observation requires either more precise measurements or higher \hat{s} .

III. RELATIONS BETWEEN COUPLINGS

The interpretation of the effective Lagrangian [Eq. 1] depends on the specified symmetry and the particle content of the underlying low-energy theory. In general, \mathcal{L}_{eff} can be expressed using either the linear or nonlinear realization of the $SU(2)_L \times U(1)_Y$ symmetry [17] to prevent unitarity violation, depending on its particle content. Thus, \mathcal{L}_{eff} can be rewritten in a form that includes the operators that describe interactions involving additional gauge bosons, and/or Goldstone bosons, and/or the Higgs field and operators of interest for any new physics effects. The number of operators can be reduced by considering their detectable contribution to the measured coupling.

Assuming the existence of a light Higgs boson, the low-energy spectrum is augmented by the Higgs doublet field ϕ , and $SU(2)_L$ and $U(1)_Y$ gauge fields. Because experimental evidence is consistent with the existence of an $SU(2)_L \times U(1)_Y$ gauge symmetry, it is reasonable to require \mathcal{L}_{eff} to be invariant with respect to this symmetry. Thus, the second term in Eq. 1 consisting of operators up to energy dimension six, is also required to have local $SU(2)_L \times U(1)_Y$ gauge symmetry and the underlying physics is described using a linear realization [18] of the $SU(2)_L \times U(1)_Y$ symmetry. By considering operators that give rise to nonstandard γWW and ZWW couplings at the tree level, \mathcal{L}_{eff} can be parametrized in terms of the α_i parameters [19]. Those parameters relate to the f_i parameters of the Lagrangian given in Eq. 1 and to the TGCs in the Lagrangian of Eq. 2 as follows [20]:

$$\begin{aligned} \Delta \kappa_\gamma &= (f_{W\phi} + f_{B\phi}) \frac{M_W^2}{2\Lambda_{NP}^2} = \alpha_{W\phi} + \alpha_{B\phi} \\ \Delta g_1^Z &= f_{W\phi} \frac{M_W^2}{2\Lambda_{NP}^2} = \Delta \kappa_Z + \frac{s_W^2}{c_W^2} \Delta \kappa_\gamma = \frac{\alpha_{W\phi}}{c_W^2} \\ \lambda &= \lambda_\gamma = \lambda_Z = 3g^2 \frac{M_W^2}{2\Lambda_{NP}^2} f_{WWW} = \alpha_W \end{aligned} \quad (5)$$

where g is the $SU(2)_L$ gauge coupling constant ($g = e/\sin\theta_W$), $c_W = \cos\theta_W$, $s_W = \sin\theta_W$, and indices $W\phi$ ($B\phi$) and W refer to operators that describe the interactions between the W (B) gauge boson field and the Higgs field ϕ , and the gauge boson field interactions, respectively. The relations in Eq. 5 give the expected order of magnitude for TGCs to be $\mathcal{O}(M_W^2/\Lambda_{NP}^2)$. Thus, for $\Lambda_{NP} \approx 2$ TeV, the expected order of magnitude for $\Delta \kappa_\gamma$, Δg_1^Z , and λ is $\mathcal{O}(10^{-3})$. This gauge-invariant parametrization, also used at LEP, gives the following relations between the $\Delta \kappa_\gamma$, Δg_1^Z and λ couplings:

$$\Delta \kappa_Z = \Delta g_1^Z - \Delta \kappa_\gamma \cdot \tan^2 \theta_W \text{ and } \lambda \equiv \lambda_Z = \lambda_\gamma \quad (6)$$

Hereafter we will refer to this relationship as the “LEP parametrization” [or $SU(2) \times U(1)$ respecting scenario] with three different parameters: $\Delta \kappa_\gamma$, λ and Δg_1^Z . The coupling $\Delta \kappa_Z$ can be expressed via the relation given by Eq. 6.

A second interpretive scenario, referred to as the equal couplings (or $ZWW = \gamma WW$) scenario [1], specifies the γWW and ZWW couplings to be equal. This is also relevant for studying interference effects between the photon and Z -exchange diagrams in WW production (see Fig. 1). In this case, electromagnetic gauge invariance forbids any deviation of g_1^γ from its SM value ($\Delta g_1^Z = \Delta g_1^\gamma = 0$) and the relations between the couplings become

$$\Delta \kappa \equiv \Delta \kappa_Z = \Delta \kappa_\gamma \text{ and } \lambda \equiv \lambda_Z = \lambda_\gamma \quad (7)$$

As already stated, for WW and WZ production the anomalous couplings contribute to the total cross section via the s -channel diagram. Anomalous couplings enter the differential production cross sections through different helicity amplitudes that depend on \hat{s} . The coupling

λ primarily affects transversely polarized gauge bosons, which is the main contribution to the total cross section. Consequently, for a given \hat{s} , the sensitivity to the coupling λ is higher than to κ because λ is multiplied by \hat{s} in dominating amplitudes for WW and WZ production. Different sensitivity to the κ couplings is expected due to the choice of scenario: the sensitivity to the κ coupling in the equal couplings scenario is higher than in the LEP parametrization scenario simply because of the different relations between Eq. 6 and Eq. 7.

IV. D0 DETECTOR

The analyzed data were produced in $p\bar{p}$ collisions at $\sqrt{s} = 1.96$ TeV by the Tevatron collider at Fermilab and collected by the D0 detector [21] during 2002 - 2006. They correspond to $1.07 \pm 0.07 \text{ fb}^{-1}$ of integrated luminosity for each of the two lepton channels ($e\nu q\bar{q}$ and $\mu\nu q\bar{q}$).

The D0 detector is a general purpose collider detector consisting of a central tracking system, a calorimeter system, and an outer muon system. The central tracking system consists of a silicon microstrip tracker and a central fiber tracker, both located within a 2 T superconducting solenoidal magnet, with designs optimized for tracking and vertexing at pseudorapidities [22] $|\eta| < 3$ and $|\eta| < 2.5$, respectively. A liquid-argon and uranium calorimeter has a central section covering pseudorapidities $|\eta|$ up to ≈ 1.1 , and two end calorimeters that extend coverage to $|\eta| \approx 4.2$, with all three housed in separate cryostats [23]. An outer muon system, covering $|\eta| < 2$, consists of a layer of tracking detectors and scintillation trigger counters in front of 1.8 T iron toroids, followed by two similar layers after the toroids [24].

Jets at D0 are reconstructed using the Run II cone algorithm [25] with cone radius $R = \sqrt{(\Delta y)^2 + (\Delta\phi)^2} = 0.5$; where y is the rapidity. Jet energies are corrected to the particle level. The jet energy resolution for data, defined as σ_{p_T}/p_T , ranges from $\sim 15\% - 25\%$ for jets with $p_T = 20$ GeV to $\sim 7\% - 12\%$ for jets with $p_T = 300$ GeV, depending on the rapidity of the jet.

The D0 detector uses a three-level trigger system for quickly filtering events from a rate of 1.7 MHz down to around 100 Hz that are stored for analysis. Events analyzed in the electron channel had to pass a trigger based on a single electron or electron+jet(s) requirement, resulting in an efficiency of $98^{+2}_{-3}\%$. The triggers based on specific single muon and muon+jet(s) requirements are about 70% efficient. Thus, all available triggers were used for the muon channel to achieve higher efficiency. We select all events that satisfy our kinematic selection requirements with no specific trigger requirement. The efficiency in this kinematic region is very nearly 100%. To estimate and account for possible biases on the shape of kinematic distributions, we compare data selected with the inclusive triggers to data selected with triggers based on a single muon. In the kinematic region of interest, the

inclusive trigger is estimated to have a shape uncertainty of less than 5% and a normalization uncertainty of 2%.

V. EVENT SELECTION AND CROSS SECTION MEASUREMENT

The analysis presented here builds upon a previous publication in which we reported the first evidence of WW/WZ production with semileptonic final states at a hadron collider [12]. Such events have two energetic jets from the hadronic decay of either a W or Z boson as well as an energetic charged lepton and significant missing transverse energy (indicating a neutrino) from the leptonic decay of the associated W boson. Therefore, at the analysis level, we selected events with a reconstructed electron or muon with transverse momentum $p_T \geq 20$ GeV and pseudorapidity $|\eta| \leq 1.1$ (2.0) for electrons (muons), a missing transverse energy of $\cancel{E}_T \geq 20$ GeV, and at least two jets with $p_T \geq 20$ GeV and $|\eta| \leq 2.5$. The jet of highest p_T was required to satisfy $p_T \geq 30$ GeV. To reduce background from processes that do not contain $W \rightarrow \ell\nu$, we required the transverse mass [26] from the lepton and \cancel{E}_T to be $M_T^{\ell\nu} \geq 35$ GeV. The multijet background, for which a jet is misidentified as a lepton, was estimated using independent data samples.

Signal (WW and WZ) and background (W +jets, Z +jets, $t\bar{t}$ and single top quark) processes were modeled using Monte Carlo (MC) simulation. All MC samples were normalized using next-to-leading-order (NLO) or next-to-next-to-leading-order predictions for SM cross sections, except the dominant background W +jets, which was scaled to match the data as described below.

In the previously published cross section measurement analysis [12], the signal and backgrounds were further separated using a multivariate classifier to combine information from several kinematic variables. The multivariate classifier chosen was a random forest (RF) classifier [27, 28]. Thirteen well-modeled kinematic variables that demonstrated a difference in probability density between signal and at least one of the backgrounds were used as inputs to the RF. The effects of systematic uncertainties on the normalization and on the shape of the RF distributions were evaluated for signal and backgrounds.

The signal cross section was determined from a fit of signal and background RF output distributions to the data by minimizing a Poisson χ^2 function (*i.e.*, a negative log likelihood) with respect to variations of the systematic uncertainties [29], assuming SM γWW and ZWW couplings. The fit simultaneously varied the WW/WZ and W +jets contributions, thereby also determining the normalization factor for the W +jets MC sample. The measured yields for signal and each background are given in Table I and the dijet mass peak extracted from data compared to the WW/WZ MC prediction is shown in Fig. 2. The combined fit of both channels to the RF output resulted in a measured cross section of

$20.2 \pm 2.5(\text{stat}) \pm 3.6(\text{syst}) \pm 1.2(\text{lumi})$ pb, which is consistent with the NLO SM predicted cross section of $\sigma(WW + WZ) = 16.1 \pm 0.9$ pb [30].

TABLE I: Measured number of events for signal and each background after the combined fit (with total uncertainties determined from the fit) and the number observed in data.

	$e\nu q\bar{q}$ channel	$\mu\nu q\bar{q}$ channel
Diboson signal	436 ± 36	527 ± 43
W +jets	10100 ± 500	11910 ± 590
Z +jets	387 ± 61	1180 ± 180
$t\bar{t}$ + single top	436 ± 57	426 ± 54
Multijet	1100 ± 200	328 ± 83
Total predicted	12460 ± 550	14370 ± 620
Data	12473	14392

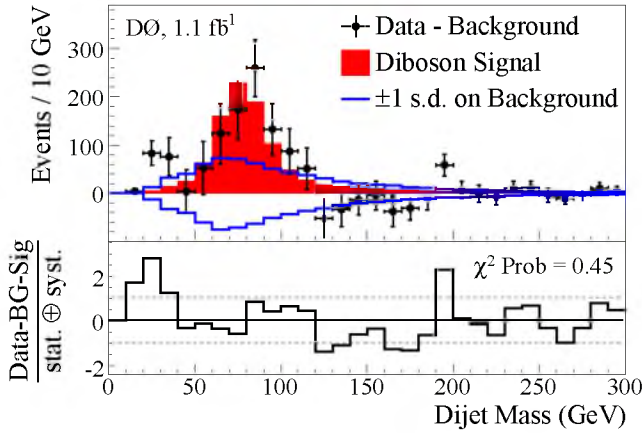


FIG. 2: A comparison of the extracted signal (filled histogram) to background-subtracted data (points), along with the ± 1 standard deviation (s.d.) systematic uncertainty on the background. The residual distance between the data points and the extracted signal, divided by the total uncertainty, is given at the bottom.

VI. SENSITIVITY TO ANOMALOUS COUPLINGS

For TGCs analysis we use the same selection and set limits on anomalous TGCs using a kinematic variable that is highly sensitive to the effects of deviations of $\Delta\kappa$, λ , and Δg_1^Z . Because TGCs introduce terms in the Lagrangian that are proportional to the momentum of the weak boson, the differential and the total cross sections will deviate from the SM prediction in the presence of anomalous couplings. This behavior is also expected at large production angles of a weak boson. Thus, the weak boson transverse momentum spectrum, p_T , is sensitive to anomalous couplings and can show a significant enhancement at high values of p_T .

The predicted WW and WZ production cross sections in the presence of anomalous TGCs are generated with

the leading order (LO) MC generator of Hagiwara, Zeppenfeld, and Woodside (HZW) [1] with CTEQ5L [31] parton distribution functions (PDFs). For example, the predicted “anomalous” cross sections relative to the SM value given by the HZW generator are shown in Fig. 3 as a function of anomalous couplings. For this figure we vary only the $\Delta\kappa$ coupling with the constraint between $\Delta\kappa_\gamma$ and $\Delta\kappa_Z$ as given by Eq. 6. The couplings λ and Δg_1^Z are fixed to their SM values (*i.e.*, $\lambda = \Delta g_1^Z = 0$). The effects of anomalous couplings on two WW kinematic distributions (p_T and rapidity of the $q\bar{q}$ system) for the LEP parametrization are shown in Fig. 4. Here again, we vary only one coupling at a time ($\Delta\kappa$, λ or Δg_1^Z) according to Eq. 6 and leave the others fixed to their SM values. Finally, we choose the $p_T^{q\bar{q}}$ (*i.e.*, reconstructed dijet p_T) distribution to be our kinematic variable to probe anomalous couplings in data. Results are interpreted in two different scenarios: LEP parametrization and equal couplings, both with $\Lambda_{NP} = 2$ TeV.

VII. REWEIGHTING METHOD

The PYTHIA [32] LO MC generator with CTEQ6L1 PDFs was used to simulate a sample of WW and WZ events at LO. We use the MC@NLO MC generator [33] with CTEQ6M PDFs to correct the event kinematics for higher order QCD effects by reweighting the differential distributions of $p_T(WV)$ and $\Delta R(W, V)$ produced by PYTHIA to match those produced via MC@NLO. We simulate the LO effects of anomalous couplings on the p_T distribution by reweighting the SM predictions for WW and WZ production from PYTHIA to include the contribution from the presence of anomalous couplings. The anomalous coupling contribution to the normalization and to the shape of $p_T^{q\bar{q}}$ distribution relative to the SM is predicted by the HZW LO MC generator.

The reweighting method uses the matrix element values given by the generator to predict an event rate in the presence of anomalous couplings. More precisely, an event rate (R) is assigned representing the ratio of the differential cross section with anomalous couplings to the SM differential cross section. Because the HZW generator does not recalculate matrix element values, we use high statistics samples to estimate the weight as a function of different anomalous couplings. Thus, we consider our approach to be a close approximation of an exact reweighting method.

The basis of the reweighting method is that, in general, the equation of the differential cross section, which has a quadratic dependence on the anomalous couplings, can be written as

$$\begin{aligned}
 d\sigma &= \text{const} \cdot |\mathcal{M}|^2 dX \\
 &= \text{const} \cdot |\mathcal{M}_{SM}|^2 \frac{|\mathcal{M}|^2}{|\mathcal{M}_{SM}|^2} dX \\
 &= \text{const} \cdot |\mathcal{M}_{SM}|^2 [1 + A(X)\Delta\kappa + B(X)\Delta\kappa^2 \\
 &\quad + C(X)\lambda + D(X)\lambda^2 + E(X)\Delta\kappa\lambda + \dots] dX \\
 &= d\sigma_{SM} \cdot R(X; \Delta\kappa, \lambda, \dots)
 \end{aligned} \tag{8}$$

where $d\sigma$ is the differential cross section that includes the contribution from the anomalous couplings, $d\sigma_{SM}$ is the SM differential cross section, X is a kinematic distribution sensitive to the anomalous couplings and $A(X)$, $B(X)$, $C(X)$, $D(X)$, and $E(X)$ are reweighting coefficients dependent on X .

In the LEP parametrization, Eq. 8 is parametrized with the three couplings $\Delta\kappa_\gamma$, λ , and Δg_1^Z and nine reweighting coefficients, $A(X) - I(X)$. Thus, the weight R in the LEP parametrization scenario is defined as

$$\begin{aligned} R(X; \Delta\kappa, \lambda, \Delta g_1) = & 1 + A(X)\Delta\kappa \\ & + B(X)(\Delta\kappa)^2 + C(X)\lambda + D(X)\lambda^2 \\ & + E(X)\Delta g_1 + F(X)(\Delta g_1)^2 + G(X)\Delta\kappa\lambda \\ & + H(X)\Delta\kappa\Delta g_1 + I(X)\lambda\Delta g_1 \end{aligned} \quad (9)$$

with $\Delta\kappa = \Delta\kappa_\gamma$, $\lambda = \lambda_\gamma = \lambda_Z$, and $\Delta g_1 = \Delta g_1^Z$.

In the equal couplings scenario, Eq. 8 is parametrized with the two couplings $\Delta\kappa$ and λ and five reweighting coefficients, $A(X) - E(X)$. In this case the weight is defined as

$$\begin{aligned} R(X; \Delta\kappa, \lambda) = & 1 + A(X)\Delta\kappa + B(X)\Delta\kappa^2 \\ & + C(X)\lambda + D(X)\lambda^2 + E(X)\Delta\kappa\lambda \end{aligned} \quad (10)$$

with $\Delta\kappa = \Delta\kappa_\gamma = \Delta\kappa_Z$ and $\lambda = \lambda_\gamma = \lambda_Z$.

The kinematic variable X is chosen to be the p_T of the $q\bar{q}$ system, which is highly sensitive to anomalous couplings, as demonstrated in Fig. 4. Depending on the number of reweighting coefficients, a system of the same number of equations allows us to calculate their values for each event. Applied on the SM distribution of X for any combination of anomalous couplings, the distribution of X weighted by R corresponds to the kinematic distribution in the presence of the given non-SM TGC.

To calculate reweighting coefficients in the LEP parametrization scenario, we generate nine different functions, F_i ($i = 1 - 9$), fitting the shape of the $p_T^{q\bar{q}}$ distributions in the presence of anomalous couplings. The values of anomalous TGCs are chosen to deviate ± 0.5 relative to the SM as shown in Table II. We calculate nine weights R_i normalizing the functions F_i with the cross sections given by the HZW generator.

TABLE II: The values of $\Delta\kappa_\gamma$, λ and Δg_1^Z used to calculate the reweighting coefficients $A(X) - I(X)$ in the LEP parametrization scenario.

	F_1	F_2	F_3	F_4	F_5	F_6	F_7	F_8	F_9
$\Delta\kappa_\gamma$	0	0	+0.5	-0.5	0	0	+0.5	+0.5	0
λ	+0.5	-0.5	0	0	0	0	+0.5	0	+0.5
Δg_1^Z	0	0	0	0	+0.5	-0.5	0	+0.5	+0.5

To verify the derived reweighting parameters, we calculated the weight R for different $\Delta\kappa$, λ , and/or Δg_1^Z values, applied the reweighting coefficients and compared

reweighted $p_T^{q\bar{q}}$ shapes to those predicted by the generator. Discrepancies in the $p_T^{q\bar{q}}$ shape of less than 5% and in normalization of less than 0.1% from those predicted by the generator represent reasonable agreement.

When measuring TGCs in the LEP parametrization, we vary two of the three couplings at a time, leaving the third coupling fixed to its SM value. This gives the three two-parameter combinations $(\Delta\kappa, \lambda)$, $(\Delta\kappa, \Delta g_1^Z)$, and $(\lambda, \Delta g_1^Z)$. For the equal couplings scenario there is only the $(\Delta\kappa, \lambda)$ combination. In each case, the two couplings being evaluated are each varied between -1 and +1 in steps of 0.01. For a given pair of anomalous coupling values, each event in a reconstructed dijet p_T bin is weighted by the appropriate weight R and all the weights are summed in that bin. The observed limits are determined from a fit of background and reweighted signal MC distributions for different anomalous couplings contributions to the observed data using the dijet p_T distribution of candidate events.

VIII. SYSTEMATIC UNCERTAINTIES

We consider two general types of systematic uncertainties. Uncertainties of the first class (TYPE I) are related to the overall normalization and efficiencies of the various contributing physical processes. The largest contributing TYPE I uncertainties are those related to the accuracy of the theoretical cross section used to normalize the background processes. These uncertainties are considered to arise from Gaussian parent distributions. The second class (TYPE II) consists of uncertainties that, when propagated through the analysis selection, impact the shape of the dijet p_T distribution. The dependence of the dijet p_T distribution on these uncertainties is determined by varying each parameter by its associated uncertainty (± 1 s.d.) and reevaluating the shape of the dijet p_T distribution. The resulting shape dependence is considered to arise from a Gaussian parent distribution. Although TYPE II uncertainties may also impact efficiencies or normalization, any uncertainty shown to impact the shape of the dijet p_T distribution is treated as TYPE II. Both types of systematic uncertainty are assumed to be 100% correlated amongst backgrounds and signals. All sources of systematic uncertainty are assumed to be mutually independent, and no intercorrelation is propagated. A list of the systematic uncertainties used in this analysis can be found in Table III.

IX. ANOMALOUS COUPLING LIMITS

The fit utilizes the MINUIT [34] software package to minimize a Poisson χ^2 with respect to variations to the systematic uncertainties [29]. The χ^2 function used is

$$\chi^2 = -2 \ln \left(\prod_{i=1}^{N_b} \frac{\mathcal{L}^P(d_i; m_i(\vec{R}))}{\mathcal{L}^P(d_i; d_i)} \prod_{k=1}^{N_s} \frac{\mathcal{L}^G(R_k \sigma_k; 0, \sigma_k)}{\mathcal{L}^G(0; 0, \sigma_k)} \right)$$

TABLE III: Systematic uncertainties in percent for Monte Carlo simulations and multijet estimates. Uncertainties are identical for both lepton channels except where otherwise indicated. The nature of the uncertainty, *i.e.*, whether it refers to a normalization uncertainty (TYPE I) or a shape dependence (TYPE II), is also provided. The values for uncertainties with a shape dependence correspond to the maximum amplitude of shape fluctuations in the dijet p_T distribution ($0 \text{ GeV} \leq p_T \leq 300 \text{ GeV}$) after ± 1 s.d. parameter changes. However, the full shape dependence is included in the calculations.

Source of systematic uncertainty	Diboson signal [%]	W +jets [%]	Z +jets [%]	Top [%]	Multijet [%]	Type
Trigger efficiency, electron channel ^a	+2/−3	+2/−3	+2/−3	+2/−3		I
Trigger efficiency, muon channel	+0/−5	+0/−5	+0/−5	+0/−5		II
Lepton identification ^a	±4	±4	±4	±4		I
Jet identification	±1	±1	±1	±<1		II
Jet energy scale	±4	±7	±5	±5		II
Jet energy resolution	±3	±4	±4	±4		I
Luminosity	±6.1	±6.1	±6.1	±6.1		I
Cross section (including PDF uncertainties)		±20	±6	±10		I
Multijet normalization, electron channel					±20	I
Multijet normalization, muon channel					±30	I
Multijet shape, electron channel					±7	II
Multijet shape, muon channel					±10	II
Diboson signal NLO/LO shape	±10					II
Diboson signal reweighting shape	±5					II
Parton distribution function (acceptance only)	±1	±3	±2	±2		II
ALPGEN η and ΔR corrections		±1	±1			II
Renormalization and factorization scale		±1	±1			II
ALPGEN parton-jet matching parameters		±1	±1			II

^a Lepton efficiencies depend on kinematics; however, their fractional uncertainties are much less kinematically dependent and have a negligible effect on the shape of the dijet p_T distribution.

$$= 2 \sum_{i=1}^{N_b} m_i(\vec{R}) - d_i - d_i \ln \left(\frac{m_i(\vec{R})}{d_i} \right) + \sum_{k=1}^{N_s} R_k^2,$$

in which the indices i and k run over the number of histogram bins (N_b) and the number of systematic uncertainties (N_s), respectively. In this function $\mathcal{L}^P(\alpha; \beta)$ is the Poisson probability for α events with a mean of β events; $\mathcal{L}^G(x; \mu, \sigma)$ is the Gaussian probability for x events in a distribution with a mean value of μ and a variance σ^2 ; R_k is a dimensionless parameter describing departures in nuisance parameters in units of the associated systematic uncertainty σ_k ; d_i is the number of data events in bin i ; and $m_i(\vec{R})$ is the number of predicted events in bin i [29].

Systematics are treated as Gaussian-distributed uncertainties on the expected numbers of signal and background events. The individual background contributions are fitted to the data by minimizing this χ^2 function over the individual systematic uncertainties [29]. The fit computes the optimal central values for the systematic uncertainties, while accounting for departures from the nominal predictions by including a term in the χ^2 function that sums the squared deviation of each systematic in units normalized by its ± 1 s.d. uncertainties.

Figure 5 shows the dijet p_T distributions in the combined electron and muon channels after the fit. The value of χ^2 is measured between data and MC dijet p_T distributions as the signal MC is varied in the presence of anomalous couplings. The $\Delta\chi^2$ values of 1 and 3.84 from

the minimum χ^2 in the parameter space, for which all other anomalous couplings are zero, represent the 68% confidence level (C.L.) and 95% C.L. limits, respectively. For the LEP parametrization, the most probable coupling values as measured in data with associated uncertainties at 68% C.L. are $\kappa_\gamma = 1.07^{+0.26}_{-0.29}$, $\lambda = 0.00^{+0.06}_{-0.06}$, and $g_1^Z = 1.04^{+0.09}_{-0.09}$. For the equal couplings scenario the most probable coupling values as measured in data with associated uncertainties at 68% C.L. are $\kappa = 1.04^{+0.11}_{-0.11}$ and $\lambda = 0.00^{+0.06}_{-0.06}$. The observed 95% C.L. limits estimated from the single parameter fit are $-0.44 < \Delta\kappa_\gamma < 0.55$, $-0.10 < \lambda < 0.11$, and $-0.12 < \Delta g_1^Z < 0.20$ for the LEP parametrization or $-0.16 < \Delta\kappa < 0.23$ and $-0.11 < \lambda < 0.11$ for the equal couplings scenario (Table IV).

The observed 68% C.L. and 95% C.L. limits in two-parameter space are shown in Figs. 6 and 7 as a function of anomalous couplings along with the most probable values of $\Delta\kappa$, λ , and Δg_1^Z .

As shown in Table V, the 95% C.L. limits on anomalous couplings $\Delta\kappa_\gamma$, $\Delta\lambda$, and Δg_1^Z set using the dijet p_T distribution of $WW/WZ \rightarrow \ell\nu jj$ events are comparable with the 95% C.L. limits set by the D0 Collaboration from WW [3], WZ [4], and $W\gamma$ [5] production in fully leptonic channels using $\approx 1 \text{ fb}^{-1}$ of data. The most recent 95% C.L. one-parameter limits from the CDF Collaboration under the equal couplings scenario at $\Lambda_{NP} = 1.5 \text{ TeV}$ are $-0.46 < \Delta\kappa < 0.39$ and $-0.18 < \lambda < 0.17$ using 350 pb^{-1} of data, combining the $\ell\nu jj$ and $\ell\nu\gamma$ ($\ell = e, \mu$) final states [6]. These re-

TABLE IV: The most probable values with total uncertainties (statistical and systematic) at 68% C.L. for κ_γ , λ , and g_1^Z along with observed 95% C.L. one-parameter limits on $\Delta\kappa_\gamma$, λ , and Δg_1^Z measured in 1.1 fb^{-1} of $WW/WZ \rightarrow \ell\nu jj$ events with $\Lambda_{NP} = 2 \text{ TeV}$.

68% C.L.	κ_γ	$\lambda = \lambda_\gamma = \lambda_Z$	g_1^Z
LEP parametrization	$\kappa_\gamma = 1.07^{+0.26}_{-0.29}$	$\lambda = 0.00^{+0.06}_{-0.06}$	$g_1^Z = 1.04^{+0.09}_{-0.09}$
Equal couplings	$\kappa_\gamma = \kappa_Z = 1.04^{+0.11}_{-0.11}$	$\lambda = 0.00^{+0.06}_{-0.06}$	
95% C.L.	$\Delta\kappa_\gamma$	$\lambda = \lambda_\gamma = \lambda_Z$	Δg_1^Z
LEP parametrization	$-0.44 < \Delta\kappa_\gamma < 0.55$	$-0.10 < \lambda < 0.11$	$-0.12 < \Delta g_1^Z < 0.20$
Equal couplings	$-0.16 < \Delta\kappa < 0.23$	$-0.11 < \lambda < 0.11$	

TABLE V: Comparison of 95% C.L. one-parameter TGC limits between the different channels studied at D0 with $\approx 1 \text{ fb}^{-1}$ of data: $WW \rightarrow \ell\nu\ell\nu$, $W\gamma \rightarrow \ell\nu\gamma$, $WZ \rightarrow \ell\ell\nu$ and $WW + WZ \rightarrow \ell\nu jj$ ($l = \mu, e$) at $\Lambda_{NP} = 2 \text{ TeV}$.

LEP parametrization	$\Delta\kappa_\gamma$	$\lambda = \lambda_\gamma = \lambda_Z$	Δg_1^Z
$WZ \rightarrow \ell\nu\ell\ell$ (1 fb^{-1})	-	$-0.17 < \lambda < 0.21$	$-0.14 < \Delta g_1^Z < 0.34$
$W\gamma \rightarrow \ell\nu\gamma$ (0.7 fb^{-1})	$-0.51 < \Delta\kappa_\gamma < 0.51$	$-0.12 < \lambda < 0.13$	
$WW \rightarrow \ell\nu\ell\nu$ (1 fb^{-1})	$-0.54 < \Delta\kappa_\gamma < 0.83$	$-0.14 < \lambda < 0.18$	$-0.14 < \Delta g_1^Z < 0.30$
$WW + WZ \rightarrow \ell\nu jj$ (1.1 fb^{-1})	$-0.44 < \Delta\kappa_\gamma < 0.55$	$-0.10 < \lambda < 0.11$	$-0.12 < \Delta g_1^Z < 0.20$
equal couplings	$\Delta\kappa_\gamma$	$\lambda = \lambda_\gamma = \lambda_Z$	Δg_1^Z
$WZ \rightarrow \ell\nu\ell\ell$ (1 fb^{-1})		$-0.17 < \lambda < 0.21$	
$W\gamma \rightarrow \ell\nu\gamma$ (0.7 fb^{-1})		$-0.12 < \lambda < 0.13$	
$WW \rightarrow \ell\nu\ell\nu$ (1 fb^{-1})	$-0.12 < \Delta\kappa < 0.35$	$-0.14 < \lambda < 0.18$	
$WW + WZ \rightarrow \ell\nu jj$ (1.1 fb^{-1})	$-0.16 < \Delta\kappa < 0.23$	$-0.11 < \lambda < 0.11$	

sults are limited by statistics, but a factor of nearly 10 times more data is expected to be available for analysis by D0 by the end of Run II of the Fermilab Tevatron. With additional data the potential to reach the individual LEP2 anomalous TGC limits [7, 8, 9] shown in Table VI is significant. The combined LEP2 results still represent the world's tightest limits on charged anomalous couplings [10] and give the most probable values of κ_γ , λ , and g_1^Z as $\kappa_\gamma = 0.973^{+0.044}_{-0.045}$, $\lambda = -0.028^{+0.020}_{-0.021}$, and $g_1^Z = 0.984^{+0.022}_{-0.019}$ at 68% C.L.

In summary, we have presented a measurement of $\gamma WW/ZWW$ couplings using a sample of semileptonic decays of WW/WZ boson pairs corresponding to 1.1 fb^{-1} of $p\bar{p}$ collisions collected with the D0 detector at the Fermilab Tevatron Collider. The measurement is in agreement with the SM. On the other hand, this analysis yields the most stringent limits on $\gamma WW/ZWW$ anomalous couplings from the Tevatron to date, complementing similar measurements performed in fully leptonic decay modes from $W\gamma$, WW , and WZ production.

TABLE VI: Measured values of κ_γ , λ and g_1^Z couplings and their associated uncertainties at 68% C.L. obtained from the one-parameter fits combining data from different topologies and energies at LEP2 experiments. The last column shows the D0 result obtained from the $\ell\nu jj$ final states only selected from 1 fb^{-1} of data. The uncertainties include both statistical and systematic sources.

68% C.L.	ALEPH	OPAL	L3	D0 ($\ell\nu jj$)
κ_γ	0.971 ± 0.063	$0.88^{+0.09}_{-0.08}$	1.013 ± 0.071	$1.07^{+0.26}_{-0.29}$
λ	-0.012 ± 0.029	$-0.060^{+0.034}_{-0.033}$	-0.021 ± 0.039	$0.00^{+0.06}_{-0.06}$
g_1^Z	1.001 ± 0.030	$0.987^{+0.034}_{-0.033}$	0.966 ± 0.036	$1.04^{+0.09}_{-0.09}$

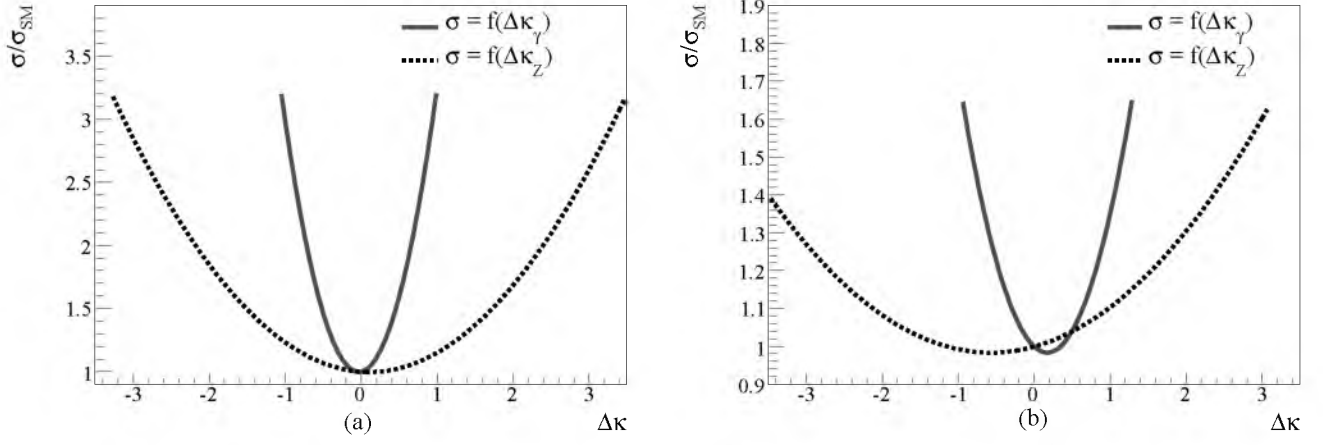


FIG. 3: Semileptonic production cross sections for (a) WW and (b) WZ normalized to the SM prediction as a function of anomalous coupling $\Delta\kappa$ ($\lambda = \Delta g_1^Z = 0$) in the LEP parametrization scenario. The new physics scale Λ_{NP} is set to 2 TeV.

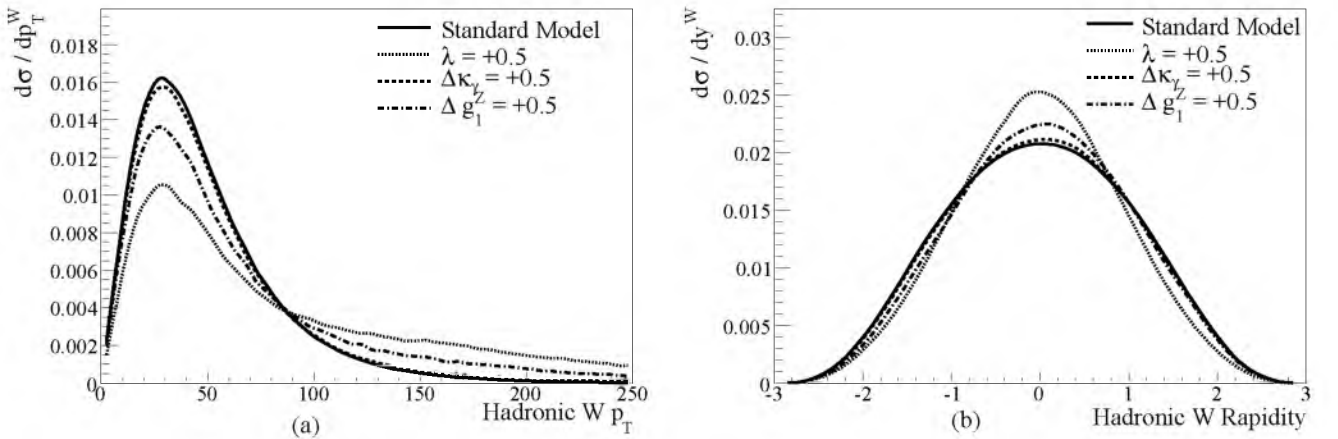


FIG. 4: Normalized distributions of the hadronic W boson (a) p_T and (b) rapidity at the parton level in WW production including anomalous couplings under the LEP parametrization scenario: $\Delta\kappa_\gamma = +0.5$ ($\lambda = \Delta g_1^Z = 0$, $\Delta\kappa_Z = -0.15$), $\lambda = +0.5$ ($\Delta\kappa_\gamma = \Delta\kappa_Z = \Delta g_1^Z = 0$), and $\Delta g_1^Z = +0.5$ ($\Delta\kappa_\gamma = \lambda = 0$, $\Delta\kappa_Z = 1.5$) compared to the SM distribution for WW production with unity normalization. The new physics scale Λ_{NP} is set to 2 TeV.

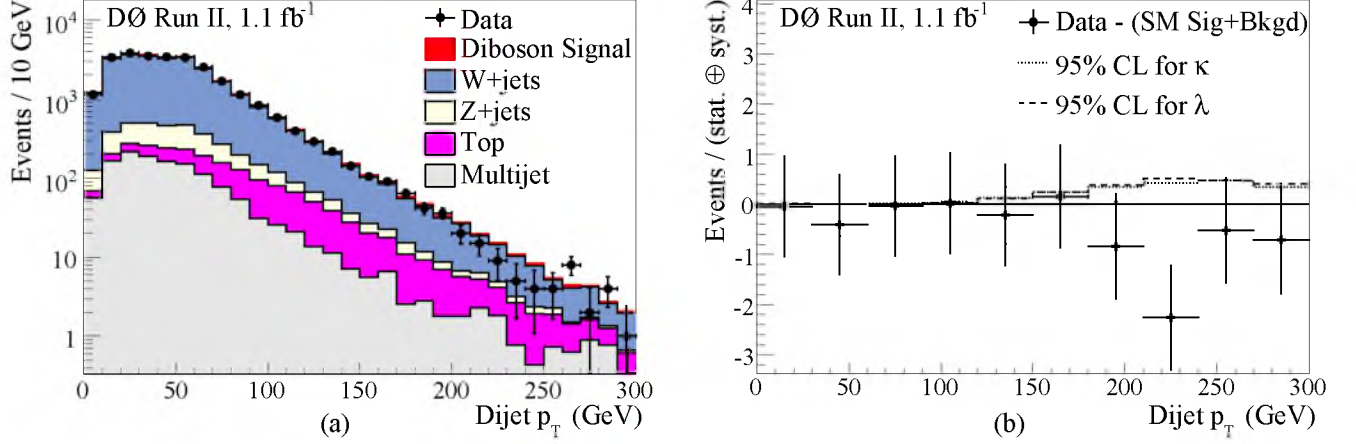


FIG. 5: (a) The dijet p_T distribution of combined (electron+muon) channels for data and SM predictions following the fit of MC to data. (b) The difference between data and simulation divided by the uncertainty (statistical and systematic) for the dijet p_T distribution. Also shown are the MC signals for anomalous couplings corresponding to the 95% C.L. limits for $\Delta\kappa$ and λ in the LEP parametrization scenario. The full error bars on the data points reflect the total (statistical and systematic) uncertainty, with the ticks indicating the contribution due only to the statistical uncertainty.

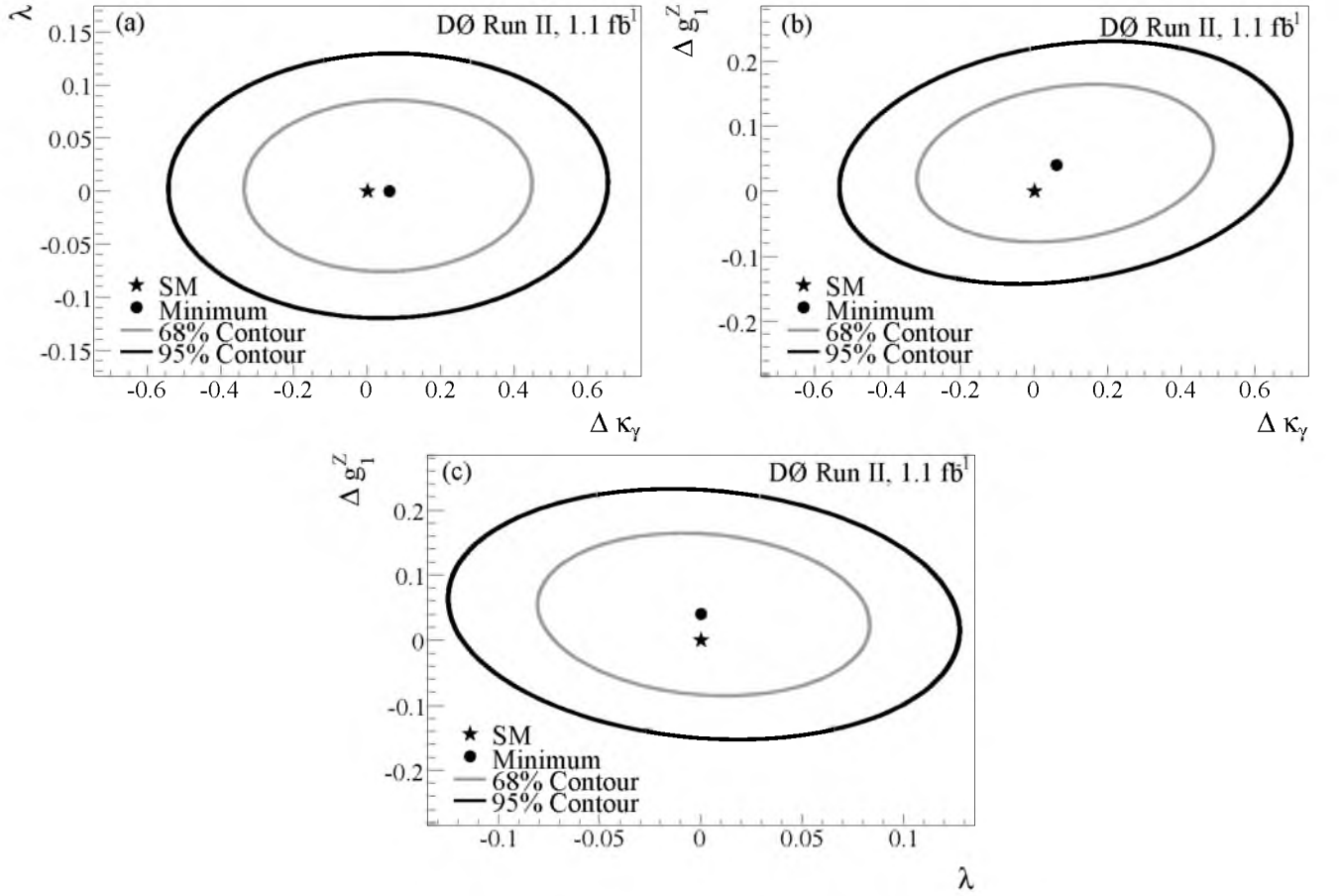


FIG. 6: The 68% C.L. and 95% C.L. two-parameter limits on the $\gamma WW/ZWW$ coupling parameters $\Delta\kappa_\gamma$, λ , and Δg_1^Z , in the LEP parametrization scenario and $\Lambda_{NP} = 2$ TeV. The dots indicate the most probable values of anomalous couplings from the two-parameter combined (electron+muon) fit and the star markers denote the SM prediction.

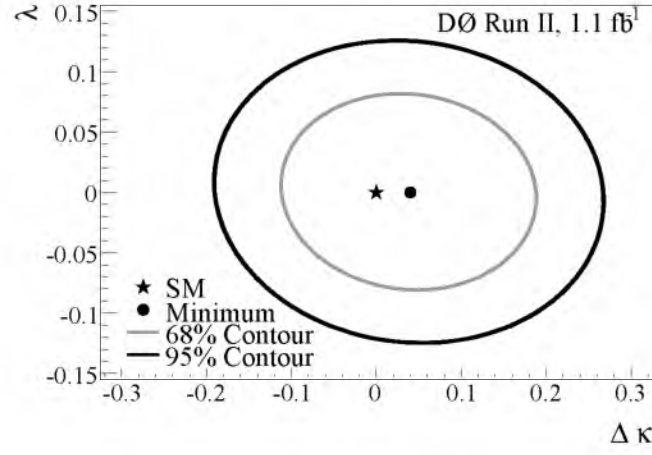


FIG. 7: The 68% C.L. and 95% C.L. two-parameter limits on the $\gamma WW/ZWW$ coupling parameters $\Delta\kappa$ and λ , in the equal couplings scenario and $\Lambda_{NP} = 2$ TeV. The dot indicates the most probable values of anomalous couplings from the two-parameter combined (electron+muon) fit and the star marker denotes the SM prediction.

We thank the staffs at Fermilab and collaborating institutions, and acknowledge support from the DOE and NSF (USA); CEA and CNRS/IN2P3 (France); FASI, Rosatom and RFBR (Russia); CNPq, FAPERJ, FAPESP and FUNDUNESP (Brazil); DAE and DST (India); Colciencias (Colombia); CONACyT (Mexico); KRF and KOSEF (Korea); CONICET and UBACyT (Ar-

gentina); FOM (The Netherlands); STFC and the Royal Society (United Kingdom); MSMT and GACR (Czech Republic); CRC Program, CFI, NSERC and WestGrid Project (Canada); BMBF and DFG (Germany); SFI (Ireland); The Swedish Research Council (Sweden); CAS and CNSF (China); and the Alexander von Humboldt Foundation (Germany).

-
- [a] Visitor from Augustana College, Sioux Falls, SD, USA.
 - [b] Visitor from Rutgers University, Piscataway, NJ, USA.
 - [c] Visitor from The University of Liverpool, Liverpool, UK.
 - [d] Visitor from Centro de Investigacion en Computacion - IPN, Mexico City, Mexico.
 - [e] Visitor from ECFM, Universidad Autonoma de Sinaloa, Culiacán, Mexico.
 - [f] Visitor from Universität Bern, Bern, Switzerland.
 - [g] Visitor from Universität Zürich, Zürich, Switzerland.
- [1] K. Hagiwara, J. Woodside, and D. Zeppenfeld, Phys. Rev. D **41**, 2113 (1990).
 - [2] S. Weinberg, Phys. Rev. D **13**, 974 (1976); L. Susskind, Phys. Rev. D **20**, 2619 (1979); H. P. Nilles, Phys. Rep. **110**, 1 (1984); H. E. Haber and G. L. Kane, Phys. Rep. **117**, 75 (1985); A. G. Cohen, D. B. Kaplan and A. E. Nelson, Phys. Lett. B **388**, 588 (1996); C. Csaki, C. Grojean, L. Pilo and J. Terning, Phys. Rev. Lett. **92**, 101802 (2004); R. Foadi, S. Gopalakrishna and C. Schmidt, JHEP **0403**, 042 (2004).
 - [3] D0 Collaboration, V. M. Abazov *et al.*, arXiv:hep-ex/0904.0673 (2009), submitted to Phys. Rev. Lett. .
 - [4] D0 Collaboration, V. M. Abazov *et al.*, Phys. Rev. D **76**, 111104(R) (2007).
 - [5] D0 Collaboration, V. M. Abazov *et al.*, Phys. Rev. Lett. **100**, 241805 (2008).
 - [6] CDF Collaboration, T. Aaltonen *et al.*, Phys. Rev. D **76**, 111103(R) (2007).
 - [7] ALEPH Collaboration, S. Schael *et al.*, Phys. Lett. B **614**, 7 (2005).
 - [8] OPAL Collaboration, G. Abbiendi *et al.*, Eur. Phys. J. C **33**, 463 (2004).
 - [9] L3 Collaboration, P. Achard *et al.*, Phys. Lett. B **586**, 151 (2004).
 - [10] LEP Collaborations ALEPH, DELPHI, L3, OPAL, and LEP TGC Working Group, Report No. LEPEWWG/TGC/2005-01 (2005).
 - [11] CDF Collaboration, D. Acosta *et al.*, Phys. Rev. Lett. **94**, 211801 (2005); A. Abulencia *et al.*, Phys. Rev. Lett. **98**, 161801 (2007); T. Aaltonen *et al.*, Phys. Rev. Lett. **100**, 201801 (2008).
 - [12] D0 Collaboration, V. M. Abazov *et al.*, Phys. Rev. Lett. **102**, 161801 (2009).
 - [13] B. W. Lee, C. Quigg, and H. B. Thacker, Phys. Rev. D **16**, 1519 (1977); W. Marciano, G. Valencia, and S. Willenbrock, Phys. Rev. D **40**, 1725 (1989); S. Dawson and S. Willenbrock, Phys. Rev. Lett. **62**, 1232 (1989).
 - [14] S. Alam, S. Dawson and R. Szalapski, Phys. Rev. D **57**, 1577 (1998).
 - [15] K. Hagiwara *et al.*, Nucl. Phys. **B282**, 253 (1987).
 - [16] U. Baur and D. Zeppenfeld, Phys. Lett. B **201**, 383 (1988).
 - [17] T. Appelquist and C. Bernard, Phys. Rev. D **22**, 200 (1980); C. N. Leung, S. T. Love and S. Rao, Z. Phys. C **31** 433 (1986).
 - [18] C. Grosse-Knetter, I. Kuss, D. Schildknecht, Phys. Lett. B **358**, 87 (1995).
 - [19] M. Bilenky, J. L. Kneur, F. M. Renard and D. Schildknecht, Nucl. Phys. **B409**, 22 (1993); Nucl. Phys. **B419**, 240 (1994); G. Gounaris *et al.*, arXiv:hep-ph/9601233 (1996); C. Grosse-Knetter, I. Kuss and D. Schildknecht, Z. Phys. C **60**, 375 (1993).
 - [20] K. Hagiwara, S. Ishihara, R. Szalapski and D. Zeppenfeld, Phys. Rev. D **48**, 2182 (1993).
 - [21] D0 Collaboration, V. M. Abazov *et al.*, Nucl. Instrum. Methods Phys. Res. A **565**, 463 (2006).
 - [22] D0 uses a cylindrical coordinate system with the z axis running along the beam axis. Angles θ and ϕ are the polar and azimuthal angles, respectively. Pseudorapidity is defined as $\eta = -\ln[\tan(\theta/2)]$, in which θ is measured with respect to the proton beam direction. In the massless limit, η is equivalent to the rapidity $y = (1/2) \ln[(E + p_z)/(E - p_z)]$. η_{det} is the pseudorapidity measured with respect to the center of the detector.
 - [23] D0 Collaboration, S. Abachi *et al.*, Nucl. Instrum. Methods Phys. Res. A **338**, 185 (1994).
 - [24] V. M. Abazov *et al.*, Nucl. Instrum. Methods Phys. Res. A **552**, 372 (2005).
 - [25] G. C. Blazey *et al.*, arXiv:hep-ex/0005012 (2000).
 - [26] J. Smith, W. L. van Neerven, and J. A. M. Vermaseren, Phys. Rev. Lett. **50**, 1738 (1983).
 - [27] L. Breiman, Machine Learning **45**, 5 (2001).
 - [28] I. Narsky, arXiv:physics/0507143 [physics.data-an] (2005).
 - [29] W. Fisher, FERMILAB-TM-2386-E.
 - [30] J. M. Campbell and R. K. Ellis, Phys. Rev. D **60**, 113006 (1999). Cross sections were calculated with the same parameter values given in the paper, except with $\sqrt{s} = 1.96$ TeV.
 - [31] J. Pumplin *et al.*, JHEP **0207**, 012 (2002).
 - [32] T. Sjöstrand *et al.*, Comput. Phys. Commun. **135**, 238 (2001).
 - [33] S. Frixione and B. R. Webber, JHEP **0206**, 029 (2002).
 - [34] F. James, "MINUIT Function Minimization and Error Analysis, Reference Manual," <http://wwwasdoc.web.cern.ch/wwwasdoc/minuit/minmain.html>